Engineering Failure Analysis 186 (2026) 110462

Contents lists available at ScienceDirect

Engineering Failure Analysis

journal homepage: www.elsevier.com/locate/engfailanal

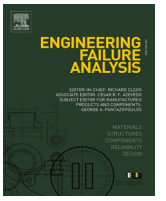

Residual mechanical capacity of small-scale partially fractured annealed laminated glass elements subjected to a quasi-static cyclic protocol

Chiara Bedon *, Riccardo Del Bello, Nicola Cella, Luca Cozzarini, Marco Fasan

University of Trieste, Department of Engineering and Architecture, Via Valerio 6/1, Trieste, Italy

ARTICLE INFO

Keywords:
Laminated glass
Annealed glass
Cyclic response
Partial fracture
Experiments
Equivalent modulus of elasticity

ABSTRACT

Ensuring appropriate levels of post-fracture security and structural safety for laminated glass (LG) elements in constructions are a primary need. Besides, these features are rather challenging to assess, due to a multitude of influencing parameters and uncertainties. As such, roughly simplified strategies are taken into account in the design of LG, to ensure suitable residual stiffness and resistance in case of possible partial damage. For safety purposes, any mechanical contribution from a cracked glass layer is fully disregarded in the analysis of the residual LG section. In this study, small-scale 2-ply LG specimens (50 mm wide × 100 mm in length) composed of annealed (AN) glass and bonded by EVA or SG interlayers are investigated. The specimens (60 in total) are subjected to randomly imposed partial fracture for one of the constituent glass layers, and tested in a three-point-bending setup in the so-called STAGE 2 (57 tests). A cyclic quasi-static protocol is imposed to the specimens, to quantify their mechanical response and partially fractured bending stiffness. The experimental results are also exploited to derive the equivalent modulus of elasticity for the cracked glass layer. In general, the experimental analysis shows a relatively stable performance of mechanical features for the given number of cycles, which suggests the availability of a minimum post-fracture capacity. However, the effect of some important influencing parameters is also highlighted.

1. Introduction

The post-fracture analysis and performance assessment of laminated glass (LG) elements is a critical task, as it has possible major consequences in terms of structural safety [1]. Besides, it is also a rather complex and uncertain issue, as it depends on many influencing parameters, such as the size of glass fragments and the interlayer characteristics [2–4], and requires complex mathematical models [5,6]. Similar considerations can be dedicated to the mechanical assessment of LG elements that are partially fractured, and represent the so-called “STAGE 2” of a typical fracture analysis, see [2,4] and Fig. 1.

In general, the performance of 2-ply LG members in bending can be described with reference to:

1) a fully elastic response in which the resistance is provided by the rotational equilibrium offered by both the glass layers;

* Corresponding author.
E-mail address: chiara.bedon@dia.units.it (C. Bedon).

https://doi.org/10.1016/j.engfailanal.2025.110462
Received 31 July 2025; Received in revised form 22 November 2025; Accepted 14 December 2025
Available online 15 December 2025

2) a partially cracked stage, in which the intact glass layer has to provide appropriate residual capacity and the broken glass ply no longer transfers bending normal stresses;
3) a third stage in which, starting from an existing defect on the glass surface of the still-intact ply, the cracks propagate inside the thickness. At this stage, the interlayer prevents the complete propagation of the crack;
4) and, finally, by a progressive increase in the severity of damage with the propagation of cracks and the gradual necking of the interlayer, up to the global collapse.

So far, several literature studies explored the post-fracture of initially intact or partially broken LG samples, pointing out the critical role of several aspects, namely represented by the type of glass (and thus the size and shape of fragments) [7,8]; the type of interlayer (and the sensitivity of its shear stiffness to environmental effects and ageing) [9–12]; the type of fracture layout (also with damage on the tensile or compressive side) [2,4,13]; the possible debonding of glass fragments from the residual LG section [14–17].

In [4], an experimental and numerical study was carried out for 2-ply partially fractured LG samples composed of annealed (AN), heat-strengthened or tempered glass (0.5 m × 1 m their size). All the samples were bonded by EVA interlayer (0.76 mm in thickness) and composed of 8 mm thick glass layers. The comparative analysis of their bending response in STAGE 2 (under small-amplitude and short-term mechanical loads) showed the capacity of the AN specimens to preserve a rather high bending stiffness (similar to that obtained for STAGE 1) when affected by fracture on the top/compressive side. For the same specimens with partial fracture on the bottom/tensile side, the bending stiffness was quantified in a −25.5 % reduction compared to the intact configuration. In any case, the AN specimens performed much better than the other samples, as a major consequence of the typical size and shape of fragments.

In this paper, the attention is focused on the experimental analysis of 2-ply AN samples characterized by a rather small size (50 mm × 100 mm), and by the presence of a pre-cracked constituent glass layer. In addition to several geometrical and mechanical configurations (including variations in glass thickness, interlayer thickness, interlayer type, displacement rate and possible artificial ageing), the attention is specifically given to the assessment of the mechanical response of the samples when subjected to a cyclic loading protocol, in order to verify and quantify a possible degradation in the examined performance indicators. More in detail, the different configurations considered in the analysis are compared in terms of initial bending stiffness, and corresponding equivalent thickness, as well as with respect to the maximum recorded force. The typical experimental observations are also addressed with the support of analytical models.

Compared to the conventional design approach (which fully disregards any broken glass layer), the present experimental investigation aims to provide some quantitative evidence about the load-bearing capacity of LG elements in a partially fractured configuration, even after being subjected to a cyclic loading protocol. Certainly, this is a rather complex topic and necessitates of multiple experimental layouts to account for the most important influencing parameters. In this sense, the presented experimental outcomes can provide technical support for possible future developments. Among others, these could even suggest a future optimization of the analysis and design process of LG cross-section, based on a partially increased post-fracture elastic mechanical capacity based on the concept of equivalent modulus of elasticity for the cracked glass layer.

2. Structural design strategy and background

As known, the structural design of LG members at the serviceability limit state (SLS) and ultimate limit state (ULS) is typically affected by strength and deflection requirements that are strongly dependent on geometrical and mechanical parameters. These include the size and aspect ratio of the LG member, the type of glass (i.e., its strength), the type of interlayer and the features of mechanical restraints (i.e., linear or point-fixing supports).

A critical step for structural safety purposes is represented by the verification of a possible partially fractured scenario, in which one of the constituent glass layers could accidentally break. This corresponds to the herein called STAGE 2, which is conventionally analysed by fully disregarding any mechanical contribution of the broken glass layer [18]. As discussed for example in [4], such a design assumption can be extremely conservative and lead to overdesign of glass elements. However, it derives from the high uncertainty that still characterizes the post-fracture performance of LG members.

The present analysis is in line with previous studies [4], but specifically addresses the cyclic residual performance and the scale effect in terms of post-fracture performance. The examined fractured scenario is markedly different from the intact configuration as in Scheme I (SI) of Fig. 2. In that case, both the glass layers can efficiently contribute to the bending capacity of the samples, according to the shear stiffness of the interlayer in use. In this context, it is useful to describe the LG section as an equivalent monolithic glass section

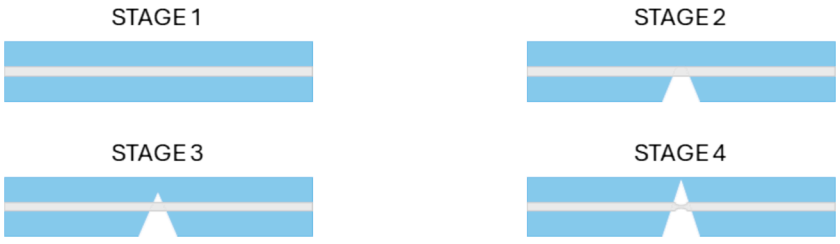

Fig. 1. Reference pre- and post-fracture stages for a 2-ply LG element.

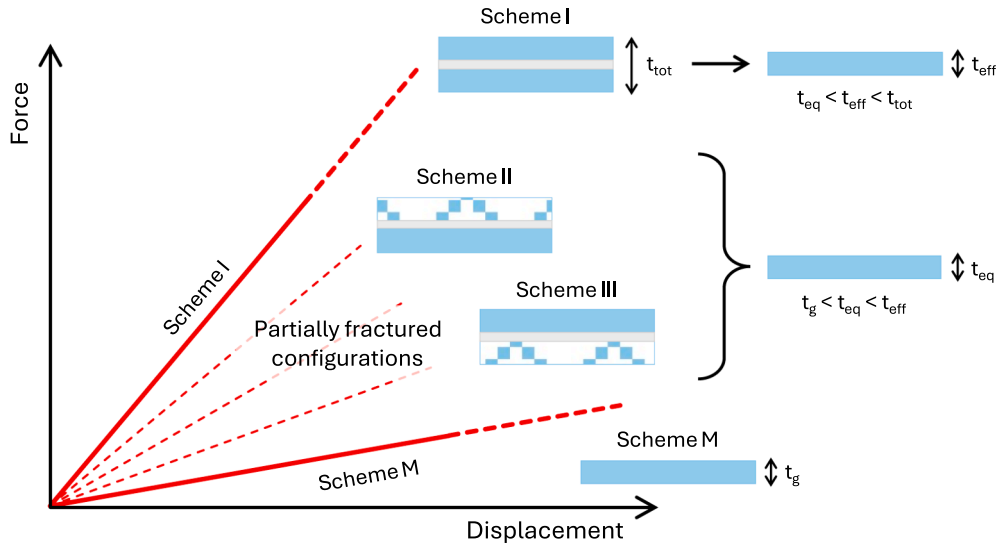

Fig. 2. Expected mechanical response for a given LG element with partial fracture.

with an effective thickness [18] in Scheme I, t_{eff}, and an equivalent thickness in partially fractured configurations, t_{eq}. According to Fig. 2, there is a clear reduction of bending stiffness in the partially fractured scenarios (Scheme II and III) compared to the SI ($t_{eq} < t_{eff}$). The present experimental investigation shows that a significant residual stiffness can be still observed for the tested samples ($t_g < t_{eq}$). This aspect is particularly emphasized when the experimental results are compared to the limit configuration that matches – in the worst case – the single intact glass layer with thickness t_g (Scheme M (SM) in Fig. 2). This outcome suggests that – even in case of partial damage – design tasks for collapse prevention could be possibly optimized, to preserve appropriate structural safety but avoiding an over-design of members. In this sense, the present study contributes to knowledge extension in the uncertain and rather complex field of post-fracture performance assessment of LG structures.

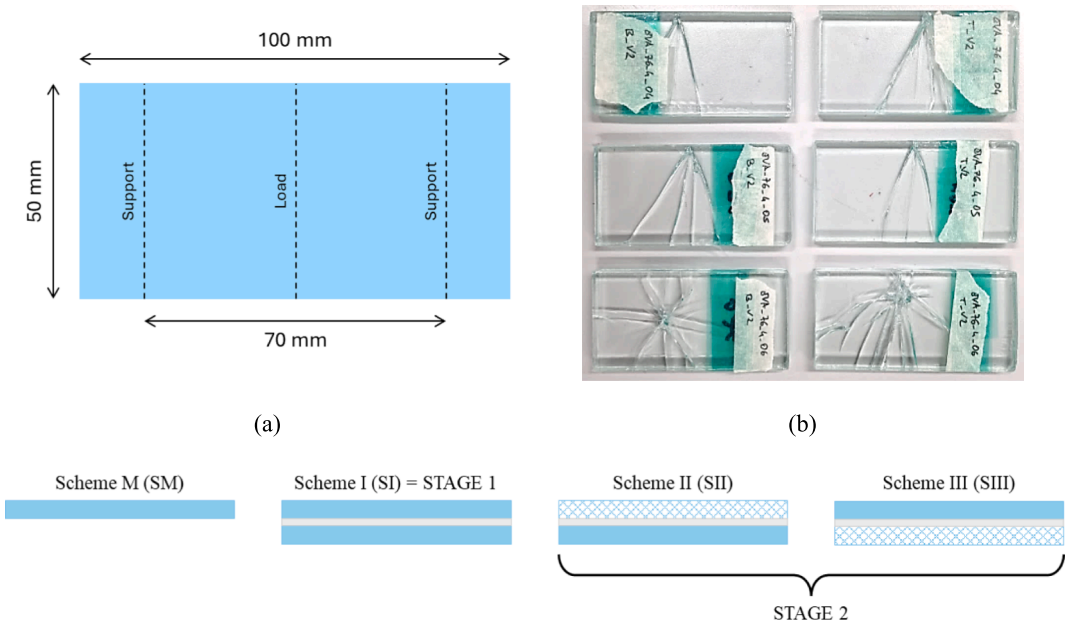

Fig. 3. Quasi-static bending tests on partially fractured AN laminated glass specimens: (a) specimen size and setup, (b) examples of pre-cracked samples (top/bottom view) and (c) cross-section of the considered configurations (pattern = broken layer).

3. Experimental investigation

An extended experimental program was carried out in laboratory conditions (at an ambient temperature of 20 ± 2°C and a relative humidity of ≈60 %), on a set of small-scale specimens, to quantify the contribution of a fractured glass layer to the overall bending stiffness of LGs in STAGE 2. The experimental tests were conducted on eight different configurations, see Section 3.1 for the composition of the LG cross-sections. At least three samples were tested for each configuration, with only one test execution per sample. The average results obtained from the test repetitions were used to compare the performance of the different configurations. The number of repetitions was reduced in case of artificial ageing, as well as in some further configurations, due to technical limitations.

3.1. Specimens

The typical specimen consisted of a 2-ply LG section, composed of two AN glass plates and a bonding polymeric interlayer. As reported in Fig. 3(a), the size of each specimen was set in 50 mm width × 100 mm length. Variations included modification of nominal glass thickness ($t_g = t_{g,nom}$ = 4 mm and 10 mm), interlayer thickness (t_{int} = 0.76 mm and 1.52 mm) and type of interlayer material (EVALAM VISUAL and SG5000 − EVA and SG respectively in the following). The governing parameters were combined to reproduce different configurations of technical interest.

Most importantly, one glass layer for each specimen was deliberately fractured by means of a steel hammer prior to the execution of bending tests, in order to facilitate the analysis of partially fractured configurations. As shown in Fig. 3(b) by the different points of origin of the cracks, the impact of the steel hammer was in a different position for each sample, resulting in randomly cracked glass elements. The attention was given, in this preliminary stage, to the definition of a through-the-thickness crack.

Different test configurations were included in the experimental program, to assess the effect of a modification in the position of the broken layer. According to Fig. 3(c), the attention was focused on the following schemes:

- Scheme II (SII): broken glass layer at the top (i.e., compressive side of the LG specimen);
- Scheme III (SIII): broken glass layer at the bottom (i.e., tensile side of the LG specimen).

Table 1 lists the key features of the examined experimental configurations.

In addition to Table 1, additional tests corresponding to SI (both glass layers intact) and to SM (a single intact glass layer) were considered for a more comprehensive comparison of experimental outcomes. For the sake of clarity, it is worth underlining that STAGE 1 in Fig. 1 and Scheme I in Fig. 3(c) represent the same configuration for a given LG element.

According to Table 1, two different displacement rates, namely 25 mm/min (V1) and 250 mm/min (V2), were employed for selected specimens to also explore the effect of loading rate, which is known to strongly affect the behaviour of the viscoelastic polymeric interlayers in use [14–17]. Moreover, the consequences of artificial ageing were also addressed for few series of specimens (see also Section 3.5).

3.2. Preliminary activities

All the specimens were first subjected to random fracture for one constituent glass layer only (Fig. 3(b)). Damage was imposed also to those specimens subjected to successive artificial ageing.

Compared to the use of artificial regular cracks, this study deliberately introduced random cracks to assess their effects on the bending response of similar samples. This means that the presented results refer to more realistic cracked scenarios, but cannot be easily replicated. Future studies will be also carried out considering additional scale effects and size aspects, to support the elaboration of specific safety factors or correction factors.

As expected, the induced fracture pattern for AN glass plates in configurations SII and SIII was characterized by the presence of few fragments, with transversal cracks running from edge to edge and through the thickness of the glass layer section. Due to the chosen manual fracturing process, the position of cracks was randomly distributed along the span of specimens, and not precisely created in the mid-span section. Two or even more fragments were in any case produced by the fracturing process (Fig. 3(b)). Considering the

Table 1
Summary of the investigated experimental configurations in STAGE 2, with evidence of the number of bending tests (57 in total).

Interlayer	t_g[mm]	t_{int}[mm]	Displacement rate [mm/min]	Scheme	Ageing	Tests
EVA	10	0.76	25 (V1), 250 (V2)	II and III	SIII	13
EVA	10	1.52	25	II and III	SII	7
EVA	4	0.76	25 and 250	II and III	–	11
EVA	4	1.52	25	II and III	–	2
SG	10	0.76	25	II and III	–	7
SG	10	1.52	25	II and III	SII	7
SG	4	0.76	25	II and III	–	5
SG	4	1.52	25	II and III	SIII	5

limited size of samples, this corresponded – for the purpose of present study – to a fully damaged constituent glass layer for the examined LG samples, as it is expected in STAGE 2.

To note that – for comparative purposes – specimens were also tested with both the glass layers intact (SI), so as to assess the reduction in performance due to the partial breakage deliberately imposed to the resisting cross-section, as listed in Table 1.

To support the analysis of experimental results – before cracking one of the glass layers and performing the bending tests – the actual average thickness of LG specimens was assessed by calliper measurements in multiple control points. As known, minor variations in the nominal thickness of glass can have major effects on their mechanical performance [19,20]. The adoption of lower glass thickness tolerance limit is recommended – though sometimes unconservative – when more precise measurements are not available [19].

For the present study, an average real thickness of about $t_{g.real} = 3.814$ mm (−4.65 %) and 9.766 mm (−2.34 %) was obtained for the glass layers in use, corresponding to LG specimens assembled with plates of nominal thickness $t_g = 4$ mm (± 0.2 mm) and 10 mm (± 0.3 mm), respectively. Moreover, the obtained $t_{g.real}$ measurements showed a rather stable trend among the available specimens. This outcome was in line with expectations, given that the small-scale specimens were produced in a single full-size LG panel and then cut into smaller parts, after lamination process.

Regarding the obtained real thicknesses and their scatter from the nominal values, this result agrees with the production tolerances prescribed by EN 572-8 [21]. However, in terms of out-of-plane bending performance considerations, it should be noted that such a scatter corresponds to a non-negligible difference, and thus should be properly considered.

3.3. Bending tests

Quasi-static displacement-controlled tests were performed on a total of 57 specimens in a simply supported configuration (beam-like setup) in STAGE 2. The typical 3-point-bending (3 PB) test configuration is shown in Fig. 4(a). During the execution of tests, both ends of LG plates were directly supported by steel blocks with rounded corners (5 mm the radius), placed 15 mm from the specimen ends. These blocks constrained the vertical displacement but allowed the rotation. Thus, the distance of supports for the 3 PB test setup resulted in 70 mm.

The vertical load was applied at the mid-span section of each LG sample through a Shimadzu AGS-X universal testing machine equipped with a rounded loading device (5 mm the radius; see Fig. 4(b)), which also recorded the force–displacement response for the tested specimen with its own data acquisition system. Test acquisitions from the machine were also integrated by preliminary background measurements based on Digital Image Correlation (DIC) techniques. In particular, the displacement components of selected LG specimens in bending were tracked by DIC during the loading stage, with a sampling rate of 0.001 s. This background step was used to cross-check the accuracy of deflection measurements.

3.4. Key performance indicators and cyclic protocol

Following the setup presented in Fig. 4, the data analysis of experimental results consisted in determining the flexural stiffness (*EI*) of the LG specimens. The actual *EI* value, in particular, was calculated by considering the out-of-plane bending response of an equivalent monolithic beam-like member. Such a formulation was found suitable for the present loading and boundary setup (i.e., Fig. 4), due to the single-axis bending response of the tested samples. However, careful consideration should be paid for the future definition and generalization of possible practical design rules, especially in consideration of the two-dimensional plate bending

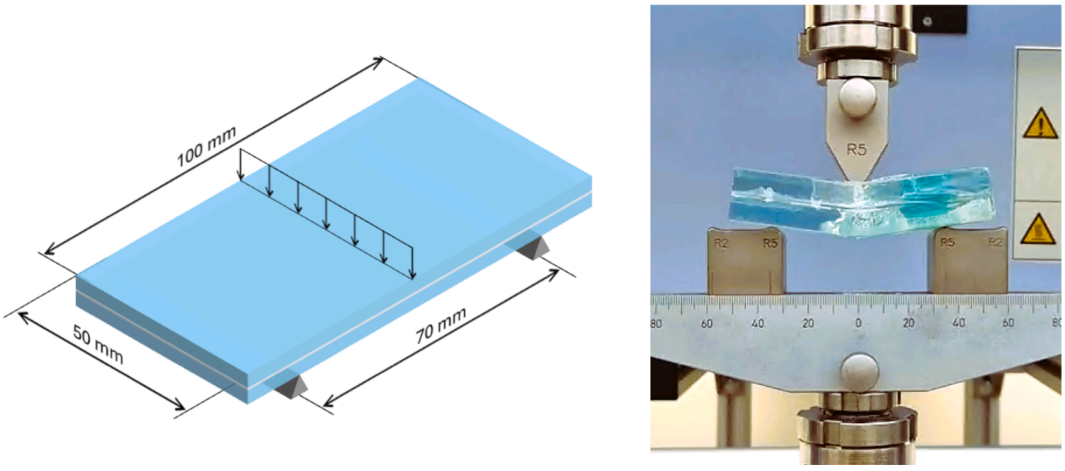

(a) (b)

Fig. 4. Typical three-point bending test: (a) schematization of test setup and (b) example of test.

behaviour that is of interest for many practical configurations for glass members. From the classical formula that describes the maximum deflection, f, of a simply supported beam with span L and subjected to a concentrated force, F, in the mid-span section:

$$f = \frac{FL^3}{48EI} \tag{1}$$

It is possible to express the corresponding flexural stiffness as:

$$EI = \frac{FL^3}{48f} \tag{2}$$

It is important to note that the so-calculated bending stiffness has the only purpose of quantitively describe the performance of each examined configuration, and to provide a simplified, but still meaningful, parameter of comparison for the mechanical performance of the tested samples.

For comparative purposes, selected mechanical parameters were quantified and compared towards their value in a reference configuration, by computing the percentage variation as:

$$\Delta P\% = \frac{P - P_{ref}}{P_{ref}} \tag{3}$$

where P is the value of a mechanical parameter in a given scheme and P_{ref} is the value of the same parameter in the reference configuration.

Based on Eq. (2), the equivalent monolithic glass thickness (t_{eq}) for the residual resisting section in SII and SIII schemes was also calculated, assuming that:

$$t_{eq} := EI = \frac{FL^3}{48f} \tag{4}$$

with $E = 70$ GPa for glass.

Most importantly, all the specimens were subjected to 20 cycles of quasi-static imposed displacement (C01-C20), in order to address any possible degradation of mechanical parameters. To this aim, the attention was focused on the analysis of a force–displacement range that is still associated to a linear elastic response of the residual glass layer. According to design standards, it is in fact expected that – in case of partial damage –the residual LG section can still provide a minimum mechanical capacity towards any possible sustained load.

Due to the high uncertainty on the actual tensile strength of AN glass (compared to the nominal characteristic value $\sigma_{t,ck} = 45$ MPa), and the need to experimentally assess the elastic response in STAGE 2, the bending experimental protocol was defined according to Fig. 5. First, the theoretical failure load $F_{u,SM}$ and the corresponding deflection $f_{u,SM}$ for the residual glass layer was analytically calculated (i.e., SM configuration), as the scenario corresponding to a maximum tensile stress $\sigma_{t,max} = \sigma_{t,ck} = 45$ MPa in the mid-span section. The so-calculated deflection $f_{u,SM}$ was then reduced by 0.5 times and considered as the reference deflection amplitude to impose the C01-C20 cycles to all the specimens. This means that a fixed deflection amplitude was used for all the specimens with $t_g = 4$ mm, and a similar approach was considered for specimens with $t_g = 10$ mm.

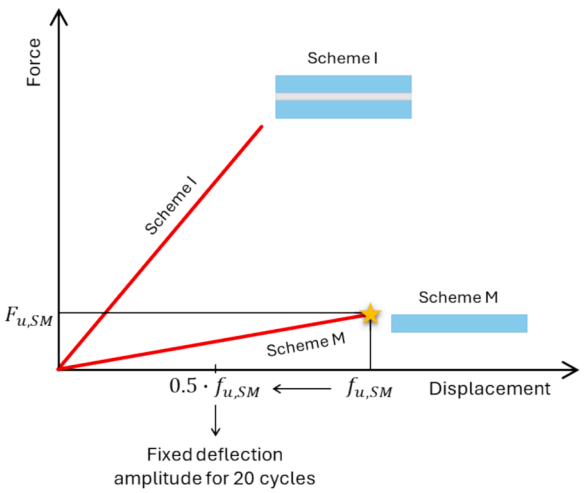

Fig. 5. Schematization of the approach for the definition of the imposed quasi-static cyclic displacement.

3.5. Artificial ageing

As specified in Table 1, an artificial ageing protocol was also considered, for a limited number of specimens, in order to compare the observed bending response with that obtained for samples subjected to possible degradation of interlayers (Fig. 6). This choice agrees with many literature studies, in which various aspects of debonding or shear stiffness have been analysed as a function of ageing and unfavourable ambient conditions, see for example [9,17,22–25].

The artificial ageing protocol was defined by drawing inspiration from the humidity test configuration prescribed by the EN 12543–4 standard [26]. The selected ageing procedure was taken into account to simulate the effects of long-term exposure to unfavourable environments, as it has major effects for laminated glass durability and load-bearing capacity. It is important to note that the artificial ageing process was carried out after subjecting the samples to the breakage of one of the constituent glass layers. Throughout the test procedure, more in detail, the specimens were kept over water in a closed container for two weeks. To ensure that all samples were adequately exposed to moisture, a set of plastic spacers were interposed to the specimens, in order to guarantee adequate spacing between them, as shown in Fig. 6(a). The temperature of the air in the container was maintained equal to 50 °C. These conditions gave a relative humidity of about 100 % and led to water condensing on the surface of the samples. The bending tests were performed within a three-hour limit at the end of the two-week period, using the setup presented in Fig. 4(b).

4. Experimental results

The elaboration of experimental results was carried out by comparing the response of specimens belonging to one series, as well as in average terms between different series, as a function of various influencing parameters. Overall, the analysis of experimental outcomes showed that – at least for the examined cyclic setup – annealed LG elements can offer relevant post-fracture bending stiffness, which is of paramount importance to possibly optimize safety levels.

4.1. Derivation of mechanical performance indicators

The attention was primarily given to the bending stiffness of the fractured LG section, as well as to the maximum force that each specimen reached under the imposed cycles. The so-collected results for samples in STAGE 2 were compared to the mechanical properties of specimens corresponding to the SI and SM configurations. Fig. 7 shows a typical example of the selected experimental results, with an imposed displacement of 0.04 mm that corresponds to ≈1/1750 the span. In this regard, it is noteworthy that the testing machine has a resolution of 0.033 μm and a precision of max (±0.1 %, ±0.01 mm), which ensured that, for the selected imposed displacement, it was possible to detect some different behaviours in the examined configurations. Minor variations were observed in the total imposed displacement, see Fig. 7, as an effect of sample adjustment and precision parameters of the machine.

More in detail, for a given force–displacement plot agreeing with Fig. 7, the bending stiffness of the fractured LG section was evaluated based on the slope of the linear path. In Fig. 7, this is represented by the segment connecting two control points on the ascending branch of each cycle. The reference force values corresponding to 10 % and 40 % of ΔF in each cycle were taken into account:

$$EI = \frac{kL^3}{48} \tag{5}$$

(a) (b)

Fig. 6. Artificial ageing: (a) preparation of pre-cracked samples for the ageing protocol and (b) climate chamber for the 2-week humidity exposure.

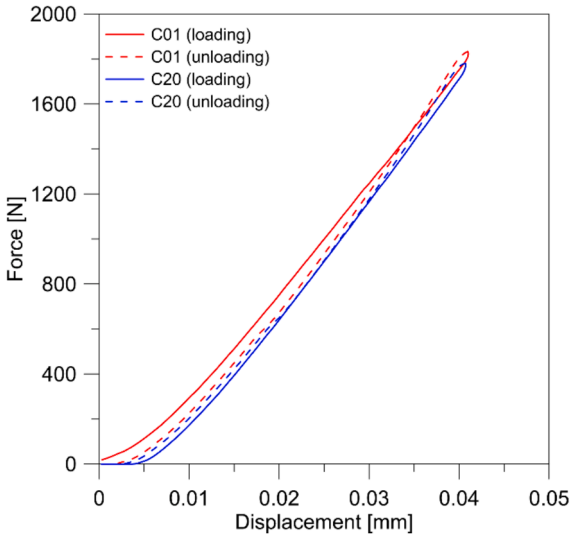

Fig. 7. Example of selected experimental results: force–displacement curve for the first (C01) and last (C20) cycles of a given specimen.

where:

$$k = \frac{F_{40} - F_{10}}{f_{40} - f_{10}} \tag{6}$$

and:

$$F_{40} = F_0 + 0.4\Delta F = F_0 + 0.4(F_{max} - F_0) \tag{7a}$$

$$F_{10} = F_0 + 0.1\Delta F = F_0 + 0.1(F_{max} - F_0) \tag{7b}$$

In Eqs. (6–7), F_{max} is the maximum force recorded during each cycle, F_0 represents the force recorded at the beginning of the cycle, while f_{40} and f_{10} are the displacements corresponding to F_{40} and F_{10}, respectively. F_0 was quantified in an average value of 28.3 N (based on all samples, all cycles and all series), and was separately calculated for Eq. (7).

The experimentally derived performance indicators are summarized in Table 2 for unaged samples tested at V1, in Table 3 for unaged samples tested at V1 and Table 4 for aged samples tested at V1. The same mean values are also depicted in Fig. 8. The results, in terms of bending stiffness of the fractured LG section, equivalent thickness and maximum force, are presented as the mean values across all cycles (C01-C20) and all the *n* specimens within each series. For this reason, the standard deviation value, σ, is also calculated for a single execution of the test ($n = 1$).

4.2. *Effect of fracture layout*

Compared to the intact specimens (Scheme I), the presence of partial fracture in STAGE 2 has major effects on the monitored bending stiffness of the composite section. In average terms, a reduction of bending stiffness in the order of −53 % and −40 % was generally observed for the 4 + 4 and 10 + 10 mm thickness configurations, respectively. Variations in terms of bending stiffness were also particularly emphasized when considering the fracture on the top/compressive (SII) or bottom/tensile (SIII) side of a given

Table 2
Mean values of maximum force (F_{max}), bending stiffness (EI) and equivalent thickness (t_{eq}) from *n* unaged specimens subjected to 20 cycles at V1.

			SII				SIII			
	t_{int} [mm]	t_g [mm]	n	$F_{max} \pm \sigma$ [N]	EI ± σ [Nm^2]	t_{eq} [mm]	n	$F_{max} \pm \sigma$ [N]	EI ± σ [Nm^2]	t_{eq} [mm]
EVA	0.76	10	2	2114 ± 152	367 ± 22	10.8	3	2269 ± 100	400 ± 27	11.1
		4	2	267 ± 34	18 ± 3	4.0	2	236 ± 10	17 ± 2	3.9
	1.52	10	2	1843 ± 56	338 ± 5	10.5	4	1937 ± 383	328 ± 65	10.4
		4	1	258 ± 3	18 ± 0	3.9	1	229 ± 2	16 ± 0	3.8
SG	0.76	10	3	2534 ± 443	447 ± 65	11.5	4	2173 ± 77	391 ± 26	11.0
		4	3	553 ± 70	36 ± 3	5.0	2	342 ± 10	26 ± 1	4.5
	1.52	10	3	1855 ± 119	353 ± 34	10.7	3	2100 ± 198	386 ± 41	11.0
		4	2	433 ± 29	29 ± 1	4.6	2	300 ± 26	22 ± 3	4.2

Table 3
Mean values of maximum force (F_{max}), bending stiffness (EI) and equivalent thickness (t_{eq}) from *n* unaged specimens subjected to 20 cycles at V2.

			SII				SIII			
	t_{int} [mm]	t_g [mm]	n	$F_{max} \pm \sigma$ [N]	EI $\pm \sigma$ [Nm^2]	t_{eq} [mm]	n	$F_{max} \pm \sigma$ [N]	EI $\pm \sigma$ [Nm^2]	t_{eq} [mm]
EVA	0.76	10	3	1702 ± 377	336 ± 74	10.5	3	1857 ± 630	354 ± 95	10.7
		4	3	250 ± 19	19 ± 1	4.0	3	205 ± 41	16 ± 2	3.8

Table 4
Mean values of maximum force (F_{max}), bending stiffness (EI) and equivalent thickness (t_{eq}) from *n* aged specimens subjected to 20 cycles at V1.

			SII				SIII			
	t_{int} [mm]	t_g [mm]	n	$F_{max} \pm \sigma$ [N]	EI $\pm \sigma$ [Nm^2]	t_{eq} [mm]	n	$F_{max} \pm \sigma$ [N]	EI $\pm \sigma$ [Nm^2]	t_{eq} [mm]
EVA	0.76	10	–	–	–	–	1	1799 ± 16	316 ± 5	10.3
	1.52	10	1	1176 ± 19	216 ± 2	9.0	–	–	–	–
SG	1.52	10	1	1936 ± 16	349 ± 8	10.6	–	–	–	–
		4	–	–	–	–	1	241 ± 6	19 ± 1	4.0

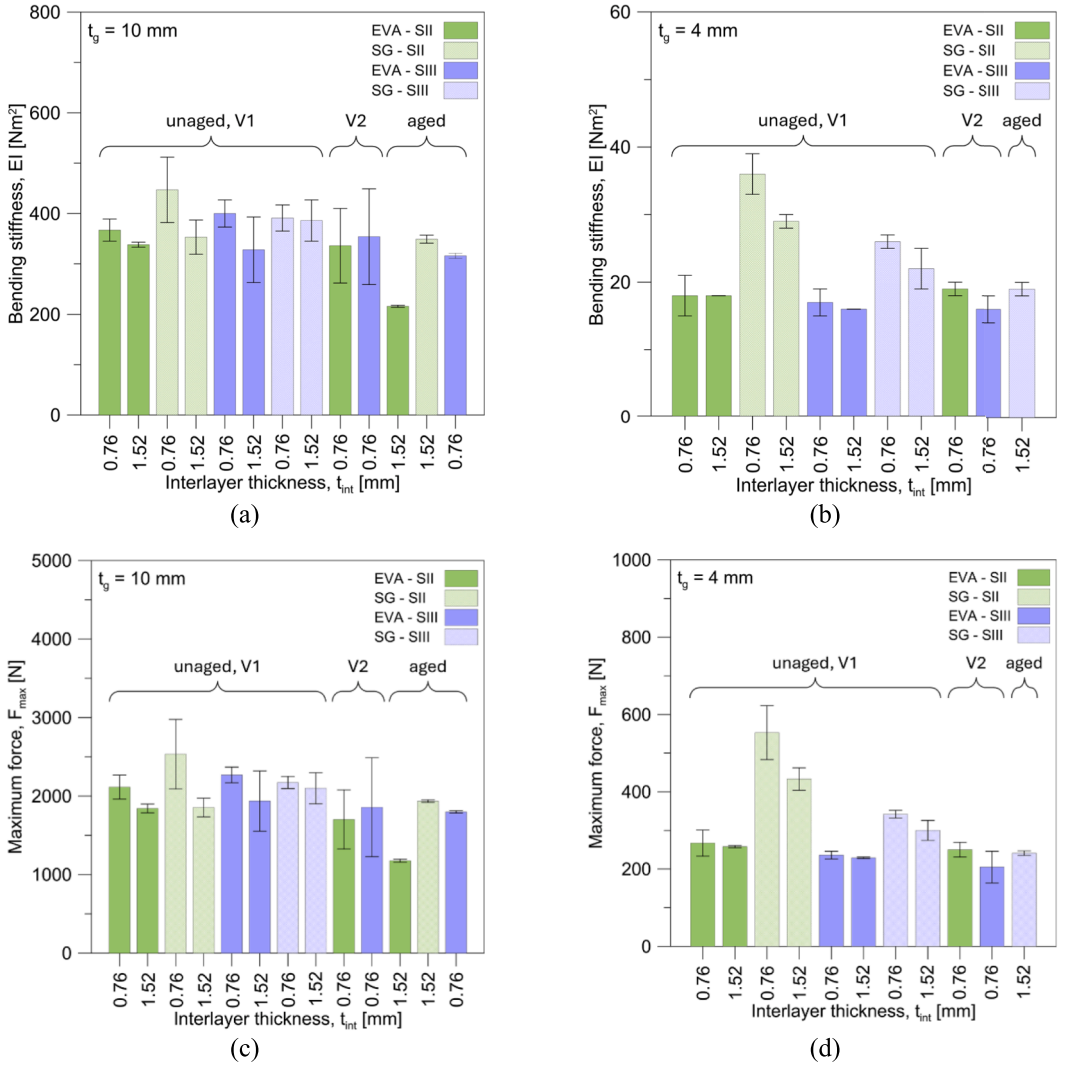

Fig. 8. Mean values of bending stiffness (EI) and maximum force (F_{max}) for (a, c) $t_g = 10$ mm and (b, d) $t_g = 4$ mm.

specimen. In general, a higher stiffness was observed in SII, due to the more significant contribution of fragments on the compressed side of the sample. However, for a few cases, the selected performance indicator was found higher in SIII. This outcome could be justified by considering the randomly imposed fracture pattern (i.e., different shape of fragments), which could affect the interlocking of fragments and its contribution to the bending stiffness.

The most important outcome is the relatively high residual bending stiffness of the tested specimens, compared to the single monolithic glass layer (SM). In practical terms, this residual stiffness and mechanical contribution of the cracked glass layer can be efficiently quantified in the form of a rather simplified approach, that is a total equivalent thickness, t_{eq}, which – according to Eq. (4) – can implicitly account for the benefit of the bonded fragments. At the same time, Δt in Table 5 expresses the percentage scatter between the experimentally derived thickness and the corresponding actual average glass thickness for SM ($t_{g,real}$) according to Eq. (3). As shown, such an equivalent glass thickness is larger than SM for all the examined configurations, both in SII and SIII.

4.3. Effect of cyclic protocol

A further analysis of the experimental results can be conducted by considering the effect of the progression of imposed cycles. This is reported in Table 6, where the bending stiffness and maximum force for the last imposed cycle (C20) are compared to their corresponding value for the first cycle (C01), SI and SM according to Eq. (3). Certainly, the presence of partial fracture reduces significantly the stiffness of the specimen compared to the SI layout. However, when the same results are compared towards the SM configuration, the marked benefit of still collaborating glass fragments can be generally seen. In particular:

- As the number of cycles increases, and therefore the number of cracks and fragments (see Fig. 9), a partial increase in the measured stiffness was observed for the majority of the tested specimens. This kind of observation, for the specific study on AN glass, can be justified by the interlocking of few fragments, in combination with the limited amplitude of the imposed cycles;
- Compared to the SI layout, the presence of a fractured glass layer led to a marked reduction of bending stiffness, which is also in line with expectations. Interestingly, this result is not negatively affected by the number of imposed cycles and suggests a certain stability in the post-fracture performance;
- When the cyclic response of partially fractured samples is assessed towards the SM configuration, finally, the interlocking of glass fragments is still emphasized by the calculated percentage variations of bending stiffness, which in most of cases are still relatively high in comparison to the limit SM condition. Such a result confirms the positive contribution of glass fragments that – as far as bonded to the interlayer – can provide a certain mechanical contribution to the residual LG section, and thus enhance the post-fracture capacity.

4.4. Effect of interlayer type

Considering that EVA and SG interlayers have a markedly different mechanical response [10,16,23], a further comparative analysis of experimental results was carried out for specimens with identical nominal geometry but characterized by a different type of interlayer.

Apparently, a stiffer bending response would be expected from SG-bonded specimens, due to the typically higher rigidity of this interlayer compared to EVA. However, such a consideration can be also affected by the randomly imposed fracture pattern, and thus by the size and shape of glass fragments and their interlocking contribution. In Table 7, ΔF_{max}, ΔEI and Δt express the percentage scatter of the experimentally derived maximum force, bending stiffness and equivalent thickness for the specimens bonded with SG compared to those bonded with EVA. The average maximum force for the assigned deflection amplitude and the bending stiffness are rather aligned with the general expectation. More precisely, in most cases, the maximum force and bending stiffness of samples with SG was found higher than those bonded by EVA. In only one of the investigated configurations, the EVA sample performed slightly better than the corresponding SG sample. This is likely attributable to the effect of the randomly imposed fracture pattern.

Table 5
Percentage variation of bending stiffness (ΔEI) and thickness (Δt) for specimens in SI, SII and SIII compared to SM. Mean values from unaged specimens subjected to 20 cycles at V1.

			SI				SII		SIII		SM	
	t_{int} [mm]	t_g [mm]	EI [Nm^2]	t_{eff} [mm]	ΔEI [%]	Δt [%]	ΔEI [%]	Δt [%]	ΔEI [%]	Δt [%]	EI [Nm^2]	$t_{g,real}$ [mm]
EVA	0.76	10	553	12.4	104	26.3	35	10.2	47	13.3	272	9.8
		4	34	4.9	111	28.8	11	5.3	5	2.6	16	3.8
	1.52	10	549	12.3	102	26.0	24	7.1	21	6.1	272	9.8
		4	34	4.9	107	28.1	11	2.6	−1	0.0	16	3.8
SG	0.76	10	764	13.8	181	40.6	65	17.3	44	12.2	272	9.8
		4	68	6.1	317	61.6	122	31.6	60	18.4	16	3.8
	1.52	10	678	13.2	149	35.2	30	9.2	42	12.2	272	9.8
		4	60	5.9	269	55.1	79	21.1	36	10.5	16	3.8

Table 6
Percentage variation of maximum force (ΔF_{max}) and bending stiffness (ΔEI) for the last imposed cycle (C20) compared to the first cycle (C01), SI and SM. Mean values from unaged specimens subjected to 20 cycles at V1.

			SII				SIII			
	t_{int}	t_g	ΔF_{max}	ΔEI			ΔF_{max}	ΔEI		
			C01	C01	SI	SM	C01	C01	SI	SM
	[mm]	[mm]	[%]	[%]	[%]	[%]	[%]	[%]	[%]	[%]
EVA	0.76	10	−3.6	17.7	−30.8	40.9	−2.4	23.4	−27.0	48.8
		4	1.9	8.4	−46.5	13.2	−0.4	8.5	−49.9	5.8
	1.52	10	−0.8	6.3	−38.3	24.8	−1.4	5.9	−39.9	21.5
		4	−6.6	−0.9	−48.2	7.7	1.9	9.1	−51.6	0.6
SG	0.76	10	−3.1	16.6	−41.1	65.6	−4.8	26.7	−48.0	46.2
		4	−2.2	−0.2	−46.6	123.1	−5.2	6.7	−61.6	60.4
	1.52	10	−3.9	35.8	−46.9	32.4	−2.2	33.8	−41.9	45.0
		4	−0.3	1.7	−52.4	75.7	−4.1	4.8	−62.6	38.1

(a) (b)

Fig. 9. Example of LG specimen: (a) with the preliminarily imposed crack and (b) after the cyclic protocol (bottom view).

Table 7
Percentage variation of maximum force (ΔF_{max}), bending stiffness (ΔEI) and equivalent thickness (Δt) for SG-bonded specimens compared to EVA-bonded specimens. Mean values from unaged specimens subjected to 20 cycles at V1.

		SII			SIII		
t_{int}	t_g	ΔF_{max}	ΔEI	Δt	ΔF_{max}	ΔEI	Δt
[mm]	[mm]	[%]	[%]	[%]	[%]	[%]	[%]
0.76	10	19.9	21.8	6.5	−4.2	−2.3	−0.9
	4	107.1	100.0	25.0	44.9	52.9	15.4
1.52	10	908.2	4.4	1.9	8.4	17.7	5.8
	4	67.8	61.1	17.9	31.0	37.5	10.5

4.5. Effect of glass and interlayer thickness

In general, the increase in glass thickness leads to a significant increment of the maximum force recorded for all the examined configurations, as shown in Table 8 for samples with 10 mm glass layers compared to those with 4 mm layers. The flexural stiffness also increases consistently, as the glass thickness increases. In contrast, Table 9 shows an opposite trend for a variation in interlayer thickness. Both the maximum load and stiffness tend to decrease as the interlayer becomes thicker. Such an outcome, although this effect is much less pronounced compared to the influence of glass thickness, confirms that the shear rigidity of the bonding connection increases as the thickness of the interlayer decreases.

4.6. Effect of imposed displacement rate

In general, as the imposed displacement rate increases (V1 = 25 mm/min to V2 = 250 mm/min, in this study) the post-fracture mechanical capacity of the tested samples decreases. Typical results are outlined in Table 10. The maximum force achieved decreases with V2 by an average of −14 % compared to the same configurations tested with V1, based on all the considered experimental results. Similar trends are observed both in SII and SIII configurations, with t_g = 4 mm and t_g = 10 mm. Maximum peaks (down to −19.5 %) are indeed recorded for the 10 mm glass specimens, which could reflect a different interlocking of fragments (both in SII and SIII).

Moreover, as reported in Table 10, both the bending stiffness and the equivalent thickness decrease as the rate increases. For the bending stiffness, the average reduction can be quantified in −5.1 % among all the tested specimens and configurations, with a peak down to −11.5 % in SIII (bottom/tensile fracture), which is the most sensitive to possible debonding of fragments, and thus to the loading speed.

The present results are even of more interest when compared to the typical response of an intact LG specimen subjected to two different displacement rates. In fact, an intact specimen is expected to show an increase in the selected performance indicators as the load rate increases. In contrast, the investigated cracked specimens revealed an opposite trend with the displacement rate, exhibiting a lesser influence from the viscoelastic behaviour of the interlayer. In this regard, the influence of the displacement rate on both the interlocking of fragments (Scheme II) and the stiffening contribution to the interlayer of fragments (Scheme III) makes the viscoelastic stiffening contribution of the interlayer negligible for cracked specimens.

In any case, the calculated equivalent thickness of glass for the residual partially fractured LG section is still higher than $t_{g,real}$ (see Tables 3 and 5), which suggests at least a minimum mechanical contribution of fragments, even with higher displacement rates. In this regard, the weakest benefit was found for the 4 mm thick specimens.

4.7. Effect of artificial ageing

As expected, artificial ageing was found to have significant effects on the observed performance indicators. Typical results are proposed in Table 11. Notably, compared to the unaged specimens, the aged samples showed in general a reduction of maximum force and even bending stiffness. Moreover, worst ageing effects were collected for the samples bonded by EVA, which is well-known to be more sensitive to humidity than SG. The comparison of results in terms of bending stiffness, see Table 11, reveals an average decrease with ageing down to −18.0 % considering all the samples and configurations. For the EVA bonded samples, this reduction can be quantified in −28.5 %, as a direct effect of interlayer degradation. This is not the case of SG bonded samples, where the bending stiffness reduces with ageing to −13.6 % in SIII and mostly vanishes (−1.1 %) for SII (fracture on the top/compressive side). Finally, the EVA bonded specimen subjected to ageing and tested in SII was probably affected by major damage, as it can be seen from the limited elastic stiffness compared to the other samples.

5. Equivalent modulus of elasticity ($E_{g,cr}$)

In conclusion, the parametric experimental results were further elaborated to derive – fitting the average experimental *EI* values of each series – the equivalent modulus of elasticity for the cracked glass layer only ($E_{g,cr}$) of the 2-ply LG section (see Table 12).

Under small-amplitude, quasi-static cyclic loads, it is reasonable to assume that debonding can be disregarded, and the mechanical contribution of AN fragments can be quantified by analysing an LG section with nominal cross-sectional features. Such an approach is

Table 8
Percentage variation of maximum force (ΔF_{max}), bending stiffness (ΔEI) and equivalent thickness (Δt) for specimens with t_g = 10 mm compared to specimens with t_g = 4 mm. Mean values from unaged specimens subjected to 20 cycles at V1.

		SII			SIII		
	t_{int} [mm]	ΔF_{max} [%]	ΔEI [%]	Δt [%]	ΔF_{max} [%]	ΔEI [%]	Δt [%]
EVA	0.76	691.8	1938.9	170.0	861.4	2252.9	184.6
	1.52	614.3	1777.8	169.2	745.9	1950.0	173.7
SG	0.76	358.2	1141.7	130.0	535.4	1403.8	144.4
	1.52	328.4	1117.2	132.6	600.0	1654.5	161.9

Table 9
Percentage variation of maximum force (ΔF_{max}), bending stiffness (ΔEI) and equivalent thickness (Δt) for specimens with $t_{int} = 1.52$ mm compared to specimens with $t_{int} = 0.76$ mm. Mean values from unaged specimens subjected to 20 cycles at V1.

		SII			SIII		
	t_g [mm]	ΔF_{max} [%]	ΔEI [%]	Δt [%]	ΔF_{max} [%]	ΔEI [%]	Δt [%]
EVA	10	−12.8	−7.9	−2.8	−14.6	−18.0	−6.3
	4	−3.4	0.0	−2.5	−3.0	−5.9	−2.6
SG	10	−26.8	−21.0	−7.0	−3.4	−1.3	0.0
	4	−21.7	−19.4	−8.0	−12.3	−15.4	−6.7

Table 10
Percentage variation of maximum force (ΔF_{max}), bending stiffness (ΔEI) and equivalent thickness (Δt) for specimens tested at V2 compared to specimens tested at V1. Mean values from unaged specimens subjected to 20 cycles.

			SII			SIII		
	t_{int} [mm]	t_g [mm]	ΔF_{max} [%]	ΔEI [%]	Δt [%]	ΔF_{max} [%]	ΔEI [%]	Δt [%]
EVA	0.76	10	−19.5	−8.4	−2.8	−18.2	−11.5	−3.6
		4	−6.4	5.6	0.0	−13.1	−5.9	−2.6

Table 11
Percentage variation of maximum force (ΔF_{max}), bending stiffness (ΔEI) and equivalent thickness (Δt) for aged specimens compared to unaged specimens. Mean values from unaged specimens subjected to 20 cycles.

			SII			SIII		
	t_{int} [mm]	t_g [mm]	ΔF_{max} [%]	ΔEI [%]	Δt [%]	ΔF_{max} [%]	ΔEI [%]	Δt [%]
EVA	0.76	10	–	–	–	−20.7	−21.0	−7.2
	1.52	10	−36.2	−36.1	−14.3	–	–	–
SG	1.52	10	4.4	−1.1	−0.9	–	–	–
		4	–	–	–	−19.7	−13.6	−4.8

Table 12
Calculated average modulus of elasticity ($E_{g,cr}$) for the cracked glass layer of unaged specimens tested at V1.

			SII		SIII	
	t_{int} [mm]	t_g [mm]	$E_{g,cr} \pm \sigma$ [GPa]	ΔE [%]	$E_{g,cr} \pm \sigma$ [GPa]	ΔE [%]
EVA	0.76	10	23.7 ± 5.4	−66.1	31.7 ± 6.7	−54.7
		4	7.6 ± 1.3	−89.1	2.7 ± 1.2	−96.1
	1.52	10	16.6 ± 1.1	−76.3	14.1 ± 15.0	−79.9
		4	5.3 ± 0.1	−92.4	0.1 ± 0.1	−99.9
SG	0.76	10	22.6 ± 8.3	−67.7	15.8 ± 3.3	−77.4
		4	22.6 ± 3.2	−67.7	11.3 ± 1.3	−83.9
	1.52	10	13.3 ± 4.6	−81.0	18.5 ± 6.6	−73.6
		4	17.5 ± 0.9	−75.0	8.7 ± 4.4	−87.6

in line with [4], where the calculated equivalent modulus for 2-ply (8 + 8) AN glass specimens bonded by EVA (500 mm × 1000 mm their size) resulted in $E_{g,cr} = 69.9$ GPa ($\Delta E = -0.1$ %) for SII and $E_{g,cr} = 37.9$ MPa ($\Delta E = -45.9$ %) in SIII. In this context, ΔE expresses the percentage variation with respect to the elastic modulus of intact glass (70 GPa).

Notably, a fractured monolithic glass layer alone has a minimum mechanical capacity, but the interlock of fragments – once allowed by other section components – can provide important mechanical benefits. This effect was shown for example in [27,28] for AN plates (40 mm × 100 mm, 6 mm in thickness) bonded by a thin anti-shatter safety film. Interestingly, the vibration frequency analysis that followed the mechanical analysis for those simply supported AN-retrofitted cracked samples subjected to repeated impacts would result – for the purpose of present study – in an average $E_{g,cr}$ equal to 32.1 GPa ($\Delta E = -54.1$ %) which is rather in close agreement with SIII results recalled from [4]. A progressive decrease in $E_{g,cr}$ was however observed with the number of imposed impacts (from an initial value of 53.4 GPa ($\Delta E = -23.7$ %), down to 10.8 GPa ($\Delta E = -84.7$ %) after the series of impacts).

For the present experimental analysis, the $E_{g,cr}$ values were derived from average test results of each series of specimens. The values

of $E_{g,cr}$, more in detail, were calculated by employing the Wölfel-Bennison model [18,30], specifically adapted to be used in the case of a LG beam with a broken layer (i.e., with two different moduli of elasticity). The method, as known, provides a value of flexural stiffness EI_{eq} which is intermediate to the stiffness of a monolithic element (i.e., ideally rigid bond and monolithic behaviour) and of a LG element with independent glass layers (i.e., weak bond and layered behaviour). This stiffness is determined by means of a linear interpolation, through a shear transfer coefficient Γ varying between zero (layered behaviour) and one (monolithic behaviour). The value of the equivalent moment of inertia I_{eq}, can thus be expressed as:

$$I_{eq} = I_g + n_E I_{cr} + \Gamma A^* d^2 \tag{8}$$

where I_g and I_{cr} are the moment of inertia of the intact and cracked glass layer, respectively, and:

$$n_E = \frac{E_{g,cr}}{E_g} \tag{9a}$$

$$A^* = \frac{A_g \bullet n_E A_{cr}}{A_g + n_E A_{cr}} \tag{9b}$$

$$d = d_g + d_{cr} \tag{9c}$$

In Eqs. (9a) to (9c), E_g is the modulus of elasticity of glass, A_g and A_{cr} are the area of the cross-section of the intact and cracked glass plate, respectively, while d_g and d_{cr} are distance of the centre of gravity (CoG) of the intact and cracked glass plate from the neutral axis of the cross-section of the laminated package, see Fig. 10. The CoG of each plate is considered in the middle plane of the plate (i.e., at half the thickness).

The position of the neutral axis from the top side of the cross-section can be calculated as follows:

$$y_n = \frac{n_E A_{cr} \bullet t_{cr}/2 + A_g \bullet \left(t_{cr} + t_{int} + t_g/2\right)}{n_E A_{cr} + A_g} \tag{10}$$

According to the original model of Wölfel [29], the shear transfer coefficient Γ, which is a measure of the transfer of shear stresses across the interlayer, is given by:

$$\Gamma = \frac{1}{1 + 9.6 \frac{t_{int} E_g I_s}{G_{int} L^2 d^2}} \tag{11a}$$

$$I_s = t_g d_g^2 + t_{cr} d_{cr}^2 \tag{11b}$$

where t_{int}, t_g and t_{cr} are the thickness of the polymeric interlayer and of the intact and cracked glass layer, respectively, G_{int} is the shear modulus of the interlayer and L is the length of the element.

It is important to note that the G_{int} values for the investigated configurations were determined from the results of preliminary experimental tests at the same displacement rate and temperature/humidity conditions. For the sake of brevity, the details of these tests are omitted. Accordingly, the reference average value for G_{int} was found to be 2.68 MPa for EVA and 67.11 MPa for SG, respectively.

Finally, the $E_{g,cr}$ value can be iteratively derived as:

$$E_{g,cr} = \frac{E_g \left(I_{eq} - I_g - \Gamma A^* d^2\right)}{I_{cr}} \tag{11}$$

Typical results are presented in Table 12 for unaged samples tested at V1, in Table 13 for unaged samples tested at V1 and Table 14 for aged samples tested at V1.

The analysis of the obtained equivalent moduli of elasticity for the cracked glass layer suggests that – among other influencing parameters – the thickness of glass has a key role in ensuring any possible mechanical interlock of fragments in the post-fracture stage. Considering both SII and SIII configurations, as well as EVA or SG interlayers, the unaged specimens subjected to V1 (see Table 12) setup can still offer – even after the imposed cyclic displacements – a minimum stiffness contribution, as it can be seen from the values presented for $t_g = 10$ mm. This effect is generally less pronounced for specimens with $t_g = 4$ mm, where close to zero equivalent moduli are also obtained. A similar trend can be seen for both 10 mm and 4 mm thick glass layers also when subjected to V2 (see Table 13),

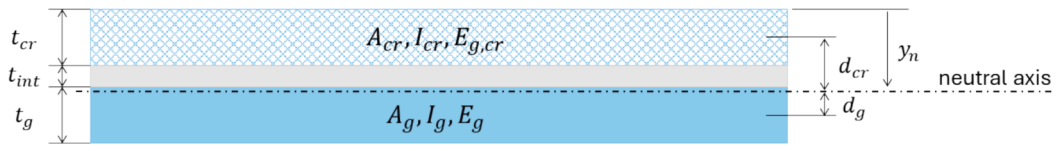

Fig. 10. Geometrical parameters for the calculation of $E_{g,cr}$.

Table 13
Calculated average modulus of elasticity ($E_{g,cr}$) for the cracked glass layer of unaged specimens tested at V2.

			SII		SII	
	t_{int} [mm]	t_g [mm]	$E_{g,cr} \pm \sigma$ [GPa]	ΔE [%]	$E_{g,cr} \pm \sigma$ [GPa]	ΔE [%]
EVA	0.76	10	25.3 ± 15.2	−63.9	36.0 ± 9.2	−48.6
		4	11.2 ± 2.9	−84.0	7.9 ± 2.1	−88.7

Table 14
Calculated average modulus of elasticity ($E_{g,cr}$) for the cracked glass layer of aged specimens tested at V1.

			SII		SIII	
	t_{int} [mm]	t_g [mm]	$E_{g,cr} \pm \sigma$ [GPa]	ΔE [%]	$E_{g,cr} \pm \sigma$ [GPa]	ΔE [%]
EVA	0.76	10	–	–	10.9 ± 1.2	−84.4
SG	1.52	10	12.7 ± 1.2	−81.9	–	–
		4	–	–	4.6 ± 0.8	−93.4

both in SII and SIII. Finally, results for aged samples (see Table 14) – whilst limited in number – are still in the order of unaged samples (excluding the EVA bonded specimen in SII), but would need further extension for statistical purposes.

In terms of possible comparative analysis of present and past experimental results, a direct correlation cannot be generalized due to the different loading setup and section layout from [4,27,28]. However, considering for example the short-term/small-amplitude loads applied in [4], some considerations can be drawn to support further studies. As shown in Table 15, the amplitude of imposed loads/displacements has a great impact on the mechanical stiffness, with a higher reduction in $E_{g,cr}$ as the load increases. Other important influencing parameters are certainly represented by the position of cracks along the span, as it is known to affect the bending stiffness and thus the overall performance of the cracked LG element [31], and by the specimen size, as observed in [32]. The closer is the crack to the mid-span section and the more severe is the degradation of mechanical capacity and bending stiffness [31]. In this study, the experiments proved that the bending stiffness of cracked LG specimens suffers for progressive modification during the imposed cyclic protocol. However, in most cases, the cracks were created close to the mid-span section (see Table 15), and the advantage of present study is also represented by the analysis of multiple samples with random crack patterns. This last assumption is aligned with the cyclic impacts explored in [27,28], where a quantitatively similar residual modulus was calculated for 100 mm long AN monolithic samples

Table 15
Qualitative comparison in terms of calculated average modulus of elasticity ($E_{g,cr}$) for the cracked glass layer based on different experimental investigations.

	Small-scale specimens (present study)	Large-scale specimen [4]
Size	50 mm × 100 mm	500 mm × 1000 mm
Deflection/span	≈ 1/1750 in SII and SIII	≈1/23000 in SII and ≈1/10600 in SIII
Imposed fracture (out-of-scale)	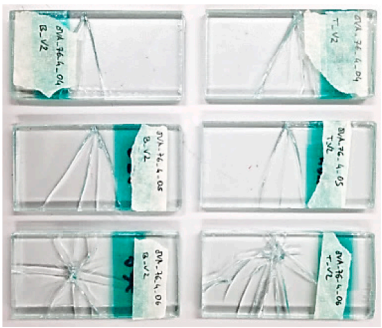	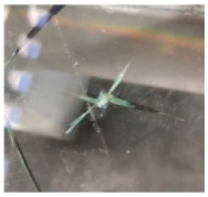 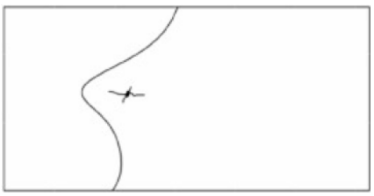

	t_{int}	t_g	SII $E_{g,cr}$	ΔE	SIII $E_{g,cr}$	ΔE	t_g	SII $E_{g,cr}$	ΔE	SIII $E_{g,cr}$	ΔE
	[mm]	[mm]	[Gpa]	[%]	[Gpa]	[%]	[mm]	[Gpa]	[%]	[Gpa]	[%]
EVA	0.76	10	23.7	−66.1	31.7	−54.7	8	69.9	−0.1	37.9	−45.9
		4	7.6	−89.1	2.7	−96.1					

($E_{g,cr}$ = 10.8 GPa). Accordingly, the number of cracks and the size of fragments confirm to have an additional implicit effect on the observed mechanical performance indicators, and should be properly considered for further extended investigations. Moreover, in [32] a further significant influence of the specimen size was observed in the post-fracture mechanical behaviour of LG plates. Consequently, subsequent experimental investigations should consider the contribution of size effect in order to extend the present findings and to correlate them to larger, real glass structures.

6. Conclusions

The post-fracture security and structural safety analysis and quantification for laminated glass elements in constructions is a critical issue, and a rather challenging task, due to many influencing parameters and aspects. Generally speaking, it is expected that the glass type (and thus the size and shape of shards) is one of the most important influencing parameters. In this paper, the attention was focused on the cyclic experimental analysis of small-scale, 2-ply LG specimens composed of AN glass. Most importantly, the experimental analysis was carried out by imposing partial fracture to one of the constituent glass layers, so as to assess the residual mechanical performance in the so-called STAGE 2 of bending response.

From a total of 60 specimens and tests, the experimental study posed the attention on different parameters, such as the interlayer type and thickness, the glass thickness, the deformation rate and the possible effect of artificial ageing. Overall. the comparative analysis gave evidence of rather interesting mechanical performances, which are certainly affected by the presence of a broken glass layer in STAGE 2, but still ensure (even under a cyclic protocol) an interesting residual capacity of the LG section, compared to the response of a single monolithic glass layer. This suggests that there is a positive and beneficial interlocking phenomenon for the glass fragments, and the LG section as a whole can take benefit of it. Thus, the present results can serve as a basis for future extended investigations and possible technical support for optimizing the safety levels of LG structural components.

CRediT authorship contribution statement

Chiara Bedon: Writing – original draft, Supervision, Project administration, Methodology, Investigation, Funding acquisition, Conceptualization. **Riccardo Del Bello:** Writing – original draft, Visualization, Validation, Formal analysis, Data curation. **Nicola Cella:** Writing – original draft, Visualization, Formal analysis, Data curation. **Luca Cozzarini:** Writing – original draft, Software, Methodology, Data curation. **Marco Fasan:** Writing – original draft, Software, Formal analysis, Data curation.

Declaration of competing interest

The authors declare that they have no known competing financial interests or personal relationships that could have appeared to influence the work reported in this paper.

Acknowledgements

These research activities are financially supported by the Italian Ministry of University and Research (MUR), via the FIS2021 Starting Grant (FIS00000609), www.hopglaz.it.

Data availability

Data will be made available on request.

References

[1] M. Feldmann, M. Laurs, J. Belis, et al., The new CEN/TS 19100: Design of glass structures, Glass Struct. Eng. 8 (2023) 317–337, https://doi.org/10.1007/s40940-023-00219-y.
[2] L. Biolzi, S. Cattaneo, M. Simoncelli, Post-failure behavior of 2-ply laminated glass plates with different interlayers, Eng. Fract. Mech. 268 (2022) 108496, https://doi.org/10.1016/J.ENGFRACMECH.2022.108496.
[3] P. Fourton, K. Piroird, M. Ciccotti, et al., Adhesion rupture in laminated glass: influence of adhesion on the energy dissipation mechanisms, Glass Struct. Eng. 5 (2020) 397–410, https://doi.org/10.1007/s40940-020-00136-4.
[4] C. Bedon, M. Kozlowski, N. Cella, Gaps in the post-breakage out-of-plane bending stiffness assessment of 2-ply partially damaged laminated glass elements under short-term quasi-static loads, Eng. Struct. 327 (2025) 119617.
[5] L. Galuppi, G. Royer-Carfagni, A homogenized model for the post-breakage tensile behavior of laminated glass, Compos. Struct. 154 (2016) 600–615.
[6] M. Seshadri, S.J. Bennison, A. Jagota, S. Saigal, Mechanical response of cracked laminated plates, Acta Mater. 50 (18) (2002) 4477–4490.
[7] L. Galuppi, G. Royer-Carfagni, The post-breakage response of laminated heat-treated glass under in plane and out of plane loading, Compos. B Eng. 147 (2018) 227–239.
[8] J. Belis, J. Depauw, D. Callewaert, D. Delincé, R. Van Impe, Failure mechanisms and residual capacity of annealed glass/SGP laminated beams at room temperature, Eng. Fail. Anal. 16 (2009) 1866–1875.
[9] L. Andreozzi, S.B. Bati, M. Fagone, G. Ranocchiai, F. Zulli, Weathering action on thermo-viscoelastic properties of polymer interlayers for laminated glass, Construct. Build Mater. 98 (2015) 757–766.
[10] T. Serafinavičius, J.-P. Lebet, C. Louter, T. Lenkimas, A. Kuranovas, Long-term laminated glass four point bending test with PVB, EVA and SG interlayers at different temperatures, Procedia Eng. 57 (2013) 996–1004.
[11] B. Liu, Y. Sun, Y. Li, Y. Wang, D. Ge, J. Xu, Systematic experimental study on mechanical behavior of PVB (polyvinyl butyral) material under various loading conditions, Polym. Eng. Sci. 52 (2012) 1137–1147.

[12] K. Machalická, M. Eliášová, Adhesive joints in glass structures: effects of various materials in the connection, thickness of the adhesive layer, and ageing, Int. J. Adhes. Adhes. 72 (Jan. 2017) 10–22, https://doi.org/10.1016/j.ijadhadh.2016.09.007.
[13] C. Zhao, J. Yang, X. Wang, I. Azim, Experimental investigation into the post-breakage performance of pre-cracked laminated glass plates, Constr. Build. Mater. 224 (2019) 996–1006.
[14] S. Chen, Z. Chen, X. Chen, J. Schneider, Evaluation of the delamination performance of polyvinyl-butyral laminated glass by through-cracked tensile tests, Constr. Build. Mater. 341 (2022) 127914.
[15] P. Elzière, C. Dalle-Ferrier, C. Creton, É. Barthel, M. Ciccotti, Large strain viscoelastic dissipation during interfacial rupture in laminated glass, Soft Matter 13 (2017) 1624–1633.
[16] X. Chen, B. Lin, M. Schuster, S. Chen, B.X. Xu, J. Schneider, Effect of moisture on the delamination properties of fractured PVB-laminated glass: a joint experimental and numerical study, Compos. Struct. 322 (2023), https://doi.org/10.1016/j.compstruct.2023.117381.
[17] A. Elkilani, A. Elsisi, H. Elemem, A. Elbelbisi, Z. Helal, H. Salim, Interlaminar bond strength of laminated glass composites under accelerated environmental effects, Construct. Build Mater. 487 (2025) 142005.
[18] CNR-DT 210/2013. Guide for the Design, Construction and Control of Buildings with Structural Glass Elements Consiglio Nazionale delle Ricerche (CNR) (2013).
[19] J Belis, C Bedon, C Louter, C Amadio, R Van Impe. Experimental and analytical assessment of lateral torsional buckling of laminated glass beams. Engineering Structures 51, 295-305.
[20] R. Kalamar, C. Bedon, M. Eliášová, Experimental investigation for the structural performance assessment of square hollow glass columns, Eng. Struct. 113 (15) (April 2016) 1–15.
[21] EN 572-8:2004. Glass in building - Basic soda lime silicate glass products - Part 8: Supplied and final cut sizes. CEN, Brussels, Belgium.
[22] UJ Udi, MM Yussof, KM Ayagi, C Bedon, MK Kamarudin. Environmental degradation of structural glass systems: A review of experimental research and main influencing parameters. Ain Shams Engineering Journal 14 (5), 101970.
[23] A. El-Sisi, M. Elsawi Mahmoud, H. El-Emam, A. Elbelbisi, H. Salim, Environmental bond degradation of different laminated glass panels, Polymers 16 (14) (2024) 2040, https://doi.org/10.3390/polym16142040.
[24] C. Butchart, M. Overend, Influence of moisture on the post-fracture performance of laminated glass, Glas. Perform. Days 2013 (2013) 59–61.
[25] X. Centelles, M. Martín, A. Solé, J.R. Castro, L.F. Cabeza, Tensile test on interlayer materials for laminated glass under diverse ageing conditions and strain rates, Constr. Build. Mater. 243 (2020) 118230.
[26] EN ISO 12543-4:2021. Glass in building - Laminated glass and laminated safety glass - Part 4: Test methods for durability (ISO 12543-4:2021). CEN, Brussels, Belgium.
[27] C. Bedon, M. Fasan, Post-fracture stiffness and residual capacity assessment of film-retrofitted monolithic glass elements by frequency change, Math. Probl. Eng. 1 (2024) 8922303.
[28] C Bedon, FA Santos. Effects of post-fracture repeated impacts and short-term temperature gradients on monolithic glass elements bonded by safety films. Composite Structures 319, 117166.
[29] E. Wölfel, Elastic composite: an approximation solution and its application possibilities, Stahlbau 6 (1987) 173–180.
[30] ASTM E1300-09a, Standard Practice for Determining Load Resistance of Glass in Buildings, American Society for Testing Material (ASTM), 2009.
[31] C. Bedon, Frequency-based early crack detection and damage severity measure in structural glass members: application to beams in bending, J. Archit. Eng. 30 (4) (2024) 04024031.
[32] S. Zhou, L. Biolzi, M. Simonceli, S. Cattaneo. Scaling Effects on Post-failure Responses of Laminated Glass Plates under Uniform Pressure. Proceedings of Glass Performance Days (GDP) 2025, 10 pages, Tampere, Finland.